

# FLUX DENSITY MEASUREMENT ON OPEN VOLUMETRIC RECEIVERS

**Felix Göhring<sup>1</sup>, Olaf Bender<sup>2</sup>, Marc Röger<sup>3</sup>, Janina Nettleau<sup>4</sup>, Peter Schwarzbözl<sup>1</sup>**

<sup>1</sup> German Aerospace Center (DLR), Solar Research, 51147 Cologne, Germany  
Phone: +49-2203 601 2994, E-Mail: felix.goehring@dlr.de

<sup>2</sup> Technical University of Darmstadt, Reactive Flows and Diagnostics, Germany

<sup>3</sup> German Aerospace Center (DLR), Solar Research, Plataforma Solar de Almería, Spain

<sup>4</sup> University of Stuttgart, Institute for Thermodynamics and Thermal Engineering, Germany

## Abstract

Flux density measurement on external receivers is an important parameter for supervision and control of commercial and research solar tower power plants. This article presents a flux density measurement system developed for open volumetric receivers that can be adapted to other receiver systems. Affordable video camera technique is used and advanced corrections are applied. Main focus is put on the challenge caused by not perfectly diffuse reflecting receiver surfaces and correction of this effect to achieve reliable measurement data. For this task the bidirectional reflectance distribution function of the used absorber material has been determined and employed. The system has been developed and tested by the German Aerospace Center (DLR) at the Plataforma Solar de Almería and the Solar Tower Jülich.

Keywords: flux density, flux distribution, bidirectional reflectance distribution function, gonioreflectometer

## 1. Introduction

Flux density measurement on external receivers is an important parameter for supervision and control of commercial and research solar tower power plants. It is a valuable input for control systems, operators, complex simulation models and is necessary for performance assessment of receiver and heliostat field. As indirect flux measurement with moving bars needs additional hardware and gets more difficult with larger receiver apertures, flux could be measured directly on the receiver surface at external receivers. Tests on the Plataforma Solar de Almería (PSA) demonstrated the feasibility of this task on small-scale receivers [1]. The technology has been applied to the Solar Power Tower Jülich (STJ), a demonstration power plant with an open volumetric receiver and nominal electric output of 1.5 MW [2], and the correction methodology has been elaborated in detail.

## 2. Indirect flux density measurement

In laboratory and test scale receivers flux measurement is often done by moving a reflecting target with Lambertian characteristics through the focus while a CCD-camera detects the reflected brightness which is proportional to the intensity of the reflected irradiation [3]. As this method needed installation of a large moving bar at the 22 m<sup>2</sup> receiver at STJ, another system was developed that basically detects the reflected radiation from the absorber surface and applies corrections and calibrations to account for the non-Lambertian characteristics and inhomogeneous reflectivities of the absorber cups.

The heliostat field of STJ consists of 2153 heliostats with almost flat mirrors and a total area of around 18 000 sqm. The control system allows free choice of aimpoints. Aiming point optimization for achieving best flux distribution during operation of the receiver at different loads is of great interest for ongoing work.

### 2.1 General setup and measurement system

The CCD-camera that captures the raw images is located between heliostat field and tower (Fig. 1) to avoid effects of retroreflection that cause difficulties to exactly quantify reflections to the camera. The receiver at STJ that is monitored by the camera consists of 1080 SiC absorber cups arranged in 36 rows and 30 columns

and each absorber cup has a front surface area of about 14 cm x 14 cm.

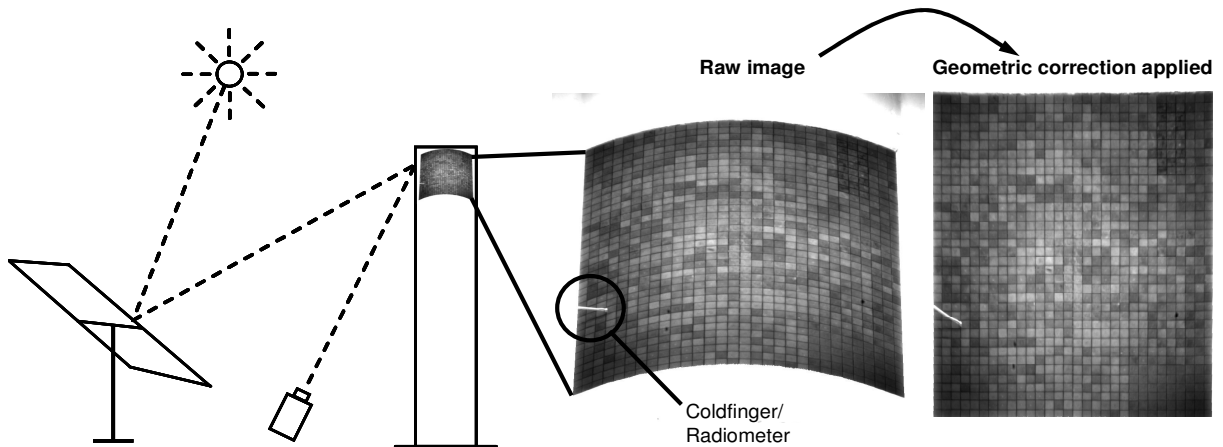


**Fig. 1: Flux measurement setup and geometric processing of raw image**

A Basler Scout scA1400-17gm camera with a 75 mm lens is used for this task. This monochrome camera is a standard industrial product with a resolution of 1392 x 1040 pixels, dynamic range of 11.2 bit and a non-linearity of less than 0.5 % (measured by the standard of the European Machine Vision Association [4]). This means that more than 2000 intensity steps can be used if exposure times are set in a way that highest intensities are still inside the linear range of the sensor signal. As highest flux densities in this application reach 1000 kW/m<sup>2</sup> flux resolution is better than 0.5 kW/m<sup>2</sup>. Another advantage of a CCD-camera as measurement system is the high possible image capture rate and continuous data acquisition without interfering with operation of the solar tower. Filters can be applied to the optics to reduce the effects of emitted thermal radiation of the heated up receiver materials to the image sensor. We showed that for an absorber surface temperature of 1200°C with an emissivity of 0.9 and an concentration factor of 500, the error caused by this reason is reduced by cutting off radiation over 0.6 μm from 0.8 % to 0.1 %. As normal maximum temperatures during operation at STJ reach 1000°C an IR-cut filter is not necessary and is not in use in this setup. Image collection, postprocessing and visualization is done with a MATLAB/Labview environment (Fig. 2).

- |   |
|---|
| 1) Aquisition of raw image                    |
| 2) Shading and dark current correction        |
| 3) Transformation (deskewing and unwinding )  |
| 4) Detection of absorber cup intensiyy values |
| 5) Ambient light correction                   |
| 6) BRDF correction                            |
| 7) Calibration with radiometer data           |
| 8) Visualization and export of results        |

**Fig. 2: Operation sequence of the measurement system**

Standard postprocessing include shading and dark current corrections. A water-cooled radiometer is mounted at the eastern side of the receiver inside a so called coldfinger (provided by Kraftanlagen München GmbH) to keep it at a constant temperature (Fig. 1). The radiometer generates live flux data which is used to calibrate the detected brightness of the processed flux distribution image [3, 5]. Due to the inertia of the radiometer every five seconds an image is captured and processed to calculate the flux distribution at the receiver aperture.

## 2.2 Postprocessing and visualization

After data collection, shading and dark current corrections are applied to the raw image [3, 5]. A transformed flat image of the receiver surface is beneficial for effective image processing. Therefore, the image is deskewed and unwinded. As the camera position and orientation is not totally stable (e.g. influence temperature and wind), the receiver corners are detected automatically for the processing of each single image. The next step is the absorber detection which assigns intensity values to each of the absorber cups. Because of a phase at the border of the absorber cups and the small gap between them the border area is not included for the calculation of the intensity values. These intensity values are computed by mean grayvalues of the remaining approx. 400 pixels of an absorber cup central area. Therefore each intensity value corresponds to an area of around 15 cm x 15 cm at the receiver surface. An example for this procedure is given in figure 3 for the calculation of the ambient light correction which is done in a similar way.

### 2.2.1 Ambient light correction

The varying reflectivities of the absorber cups are included using a correction matrix (Fig. 3). To get this matrix, the receiver surface has to be illuminated homogeneously or with a known flux distribution. Authors worked with ambient light at different meteorological conditions (clouds), because tests with artificial light by spotlights did not lead to sufficient results. This task has to be repeated regularly as aging effects alter the reflectivity of the absorber cups but also when parts of the absorber cups are replaced due to revisions etc..

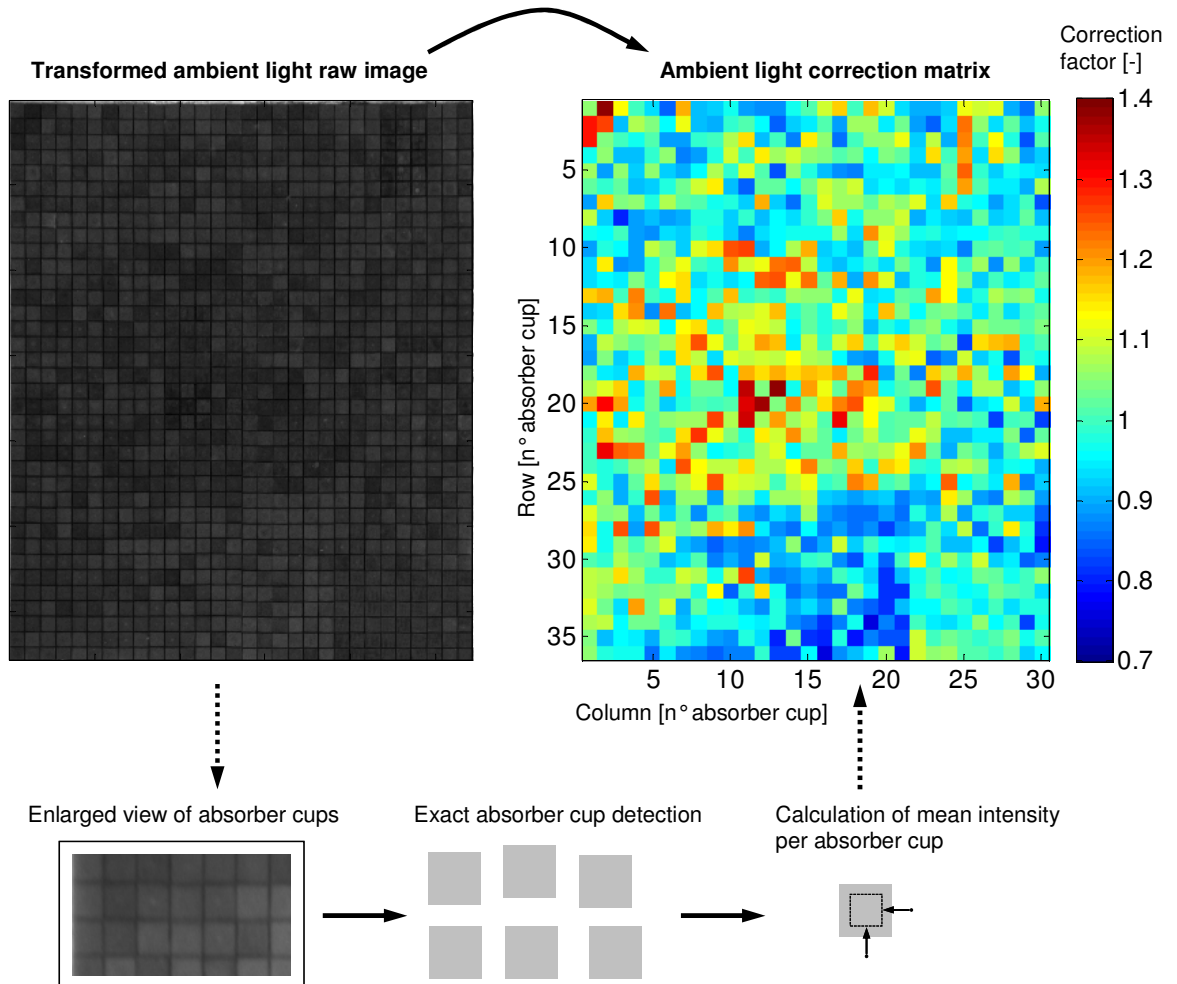


**Fig. 3: Calculation of ambient light correction matrix**

### 2.2.2 Bidirectional reflectance function correction

Another correction has to be applied to account for the influences of the different irradiation angles on the absorber cups and the non-Lambertian reflection characteristics of the structured absorber surface. The

bidirectional reflectance distribution function (BRDF) is constant for perfect diffuse reflecting materials but for real surfaces it depends on ray incidence angles and observation angles. The BRDF is a four dimensional function that is defined as the ratio between incidence and reflected radiance [6, 7]:

$$\rho(\theta, \varphi, \theta_r, \varphi_r) = \frac{L_r(\theta, \varphi, \theta_r, \varphi_r)}{L(\theta, \varphi) \cos \theta d\Omega}$$

The unit of BRDF is  $[\text{sr}^{-1}]$ . As in this work the BRDF values are only compared to those determined with the same device the raw sensor signals are used for calculations and presentations and the sensor unit [mV] is omitted.

Ray incidence zenith and azimuth angles are denoted  $\theta$  and  $\varphi$  and the corresponding reflected or observer angles are  $\theta_r$  and  $\varphi_r$ . Some authors prefer elevation instead of zenith angle, the relation is *elevation* =  $90^\circ$  - *zenith* (Fig. 4).

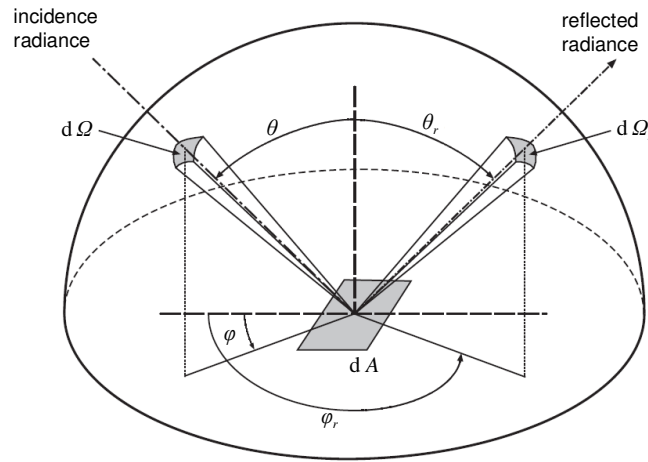


**Fig. 4: Geometry of reflections [7]**

Measurements to determine the BRDF of the applied ceramic absorber cups were carried out at DLR . For this task a gonioreflectometer (GoRef) is in use at the Institute of Solar Research in Cologne. A gonioreflectometer mainly consist of a light source and a detector that captures light reflected by the illuminated material. Zenith angles and azimuth angles of source and detector can be chosen freely. Control software of the used GoRef was adapted to automatically measure any sets of user-defined angle combinations.

Finally, a correction matrix has been developed that takes the position of each of the absorber cups and the heliostat positions into account. As the absorber cups are mounted in an cylindrical receiver that is tilted several degrees to the ground (Fig. 5) the combination of this geometry and all possible positions result for the STJ in almost 2.4 million pairs of angles that had to be evaluated with the GoRef. Similar zenith and azimuth angle groups (rounded to multiples of  $5^\circ$ ) as well as symmetries have been identified to reduce complexity of the correction matrix. Thus the number of the necessary measurements was cut down to 7186 angle combinations. Measured ranges include observer zenith and azimuth angles from  $50^\circ$  to  $60^\circ$  and  $0^\circ$  to  $25^\circ$  respectively light source zenith angles of  $0^\circ$  to  $85^\circ$  and azimuth angles from  $-180^\circ$  to  $180^\circ$ .

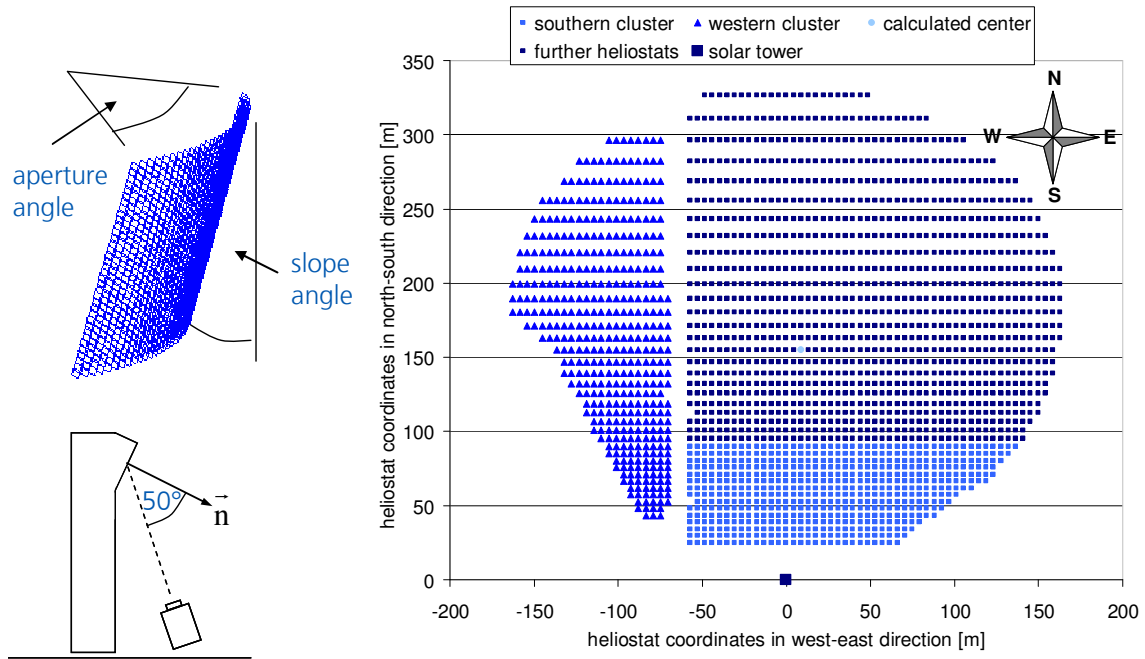


**Fig. 5: Influence of receiver geometry, camera position and heliostat field layout on observer and radiation source angles**

Figures 6 and 8 show results of relevant BRDF values according to the specific observer angles and are compared to the frequency distribution of the reduced set of angle combinations. Observer position for figures 6 and 7 corresponds to a zenith of  $50^\circ$  and azimuth of  $5^\circ$  and for figures 8 and 9 it is  $60^\circ$  and  $20^\circ$ . The plotted BRDF values of figures 6 and 7 belong to 15.56 % of those 2.4 million angle combinations while the more extreme observer angles of figures 8 and 9 show 2.59 %. It can be seen that the majority of the required measurements is in the area with almost constant BRDF values. The results demonstrate that choosing the camera position between heliostat field and tower avoids critical retroreflection angles where observer and light source angles are equal and thus block each other during measurements of BRDF. Even though BRDF measurements are influenced by this, the effect on the BRDF correction is marginal as the predominant part of relevant angle combinations are in the BRDF area without blocking effects as can be seen in direct comparison of figures 6 to 7 and 8 to 9.

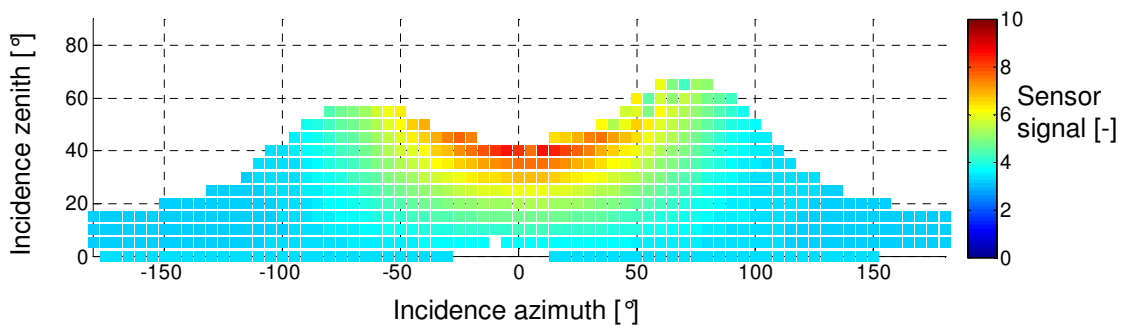


**Fig. 6: BRDF for observer zenith of  $50^\circ$  and azimuth of  $5^\circ$**

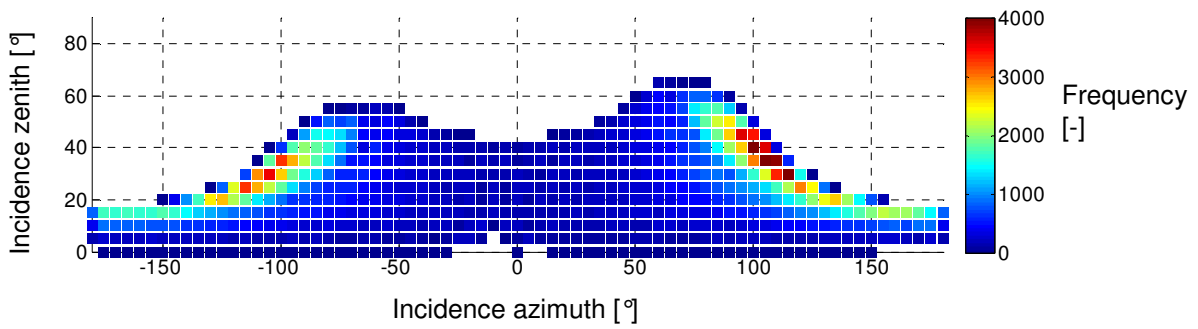


**Fig. 7: Frequency distribution for observer zenith of 50° and azimuth of 5°**

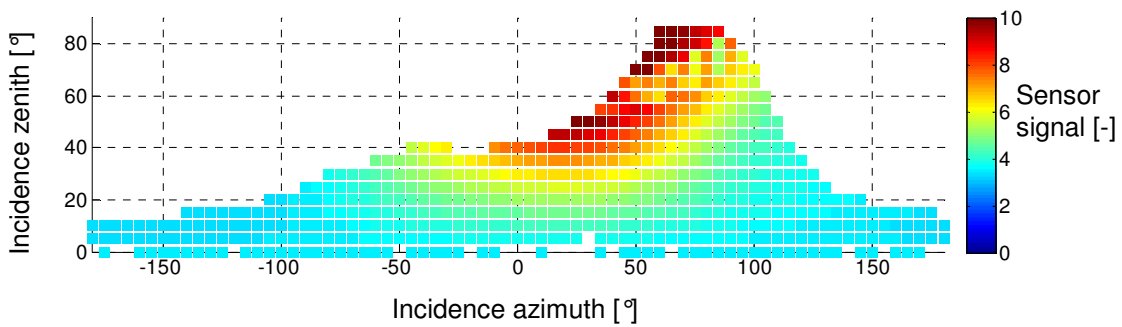


**Fig. 8: BRDF for observer zenith of 60° and azimuth of 20°**

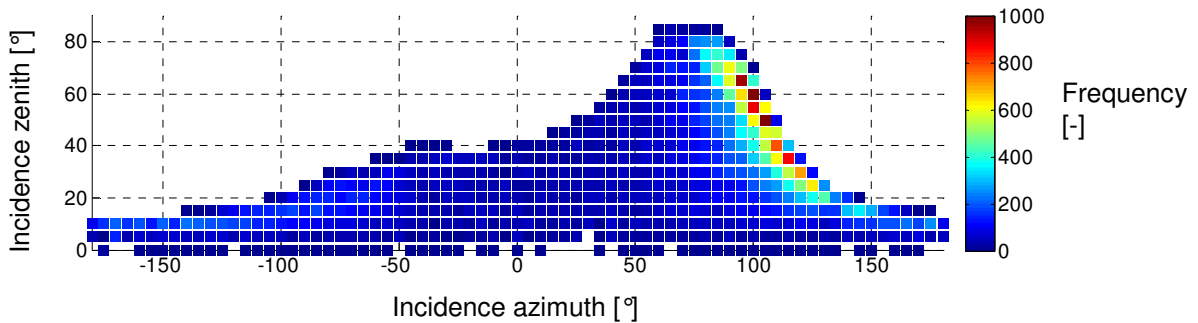


**Fig. 9: Frequency distribution for observer zenith of 60° and azimuth of 20°**

Based on this data set of BRDF values, correction matrices have been derived for different states of power plant operation. Figures 10 and 11 show four examples of those correction matrices. The relevant parts of the heliostat field are marked in figure 5. Areas of the receiver where a correction factor of over one is calculated would be underrated by the measurement system without adjustment. For areas of the receivers surface with a correction factor of less than one the opposite is true. Correction factors vary between 0.829 and 1.111 for the complete field and 0.840 and 1.114 for the center of the field at 154 m north and 9 m east of the center of receiver (Fig. 10), between 0.800 and 1.116 for the southern part and 0.672 and 1.193 for the western part (Fig. 11). The center of the heliostat field was calculated with the raytracing software STRAL [8] for varying times and is considered the source of the radiation. It is compared against the more precise correction matrix where each heliostat is a source of radiation. Maximum differences for the corrections in comparison to the application of one matrix for the complete field is up to 3.2 % for the center of the field, 6.9 % for the southern heliostat field and 30.6 % for the western part. This shows that for a correct flux distribution, used parts of the heliostat field have to be known and logged. Even the simplification to only use the center of the field as source of concentrated solar radiation leads to errors that should be prevented. If done so, solar input to the central top part of the receiver would be overestimated and to the lower edges underestimated. For the other two setups the difference for choosing the correction matrix for the complete fields leads to errors that are not tolerable for further usage of the flux distribution in e.g. simulation models or efficiency calculations.

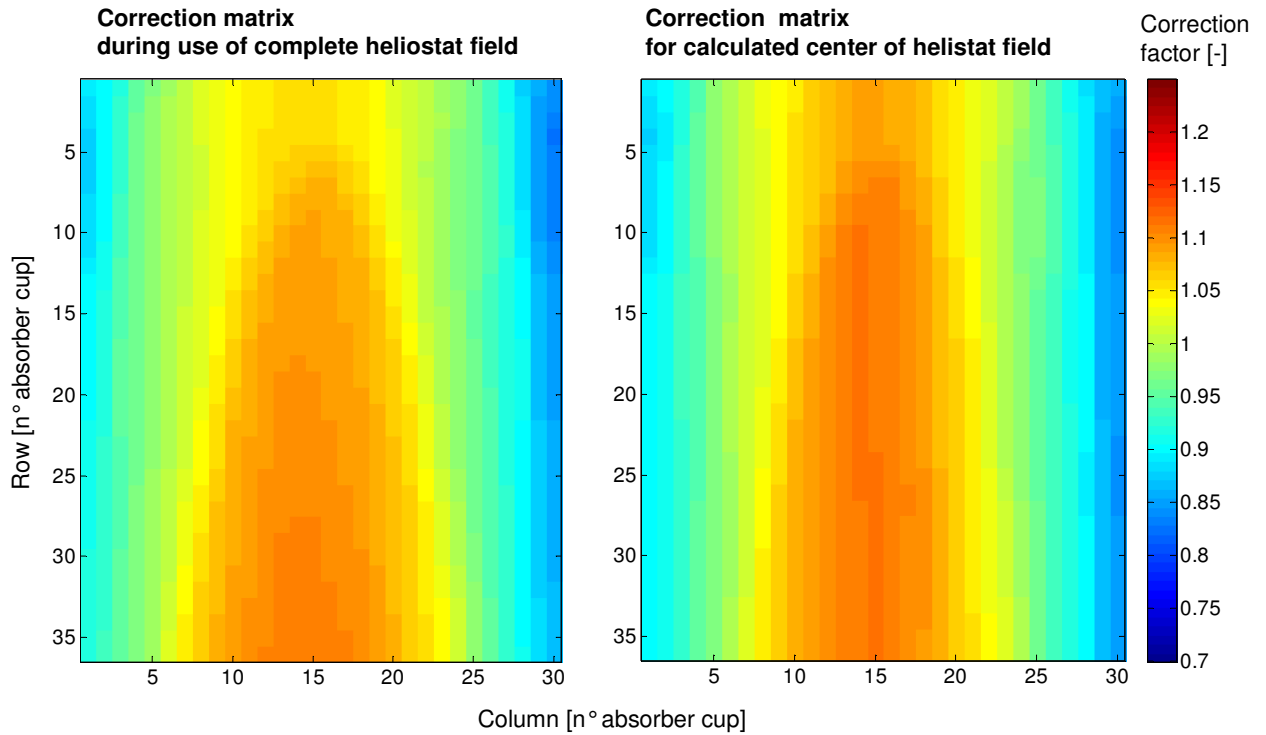


**Fig. 10: Different correction matrices**

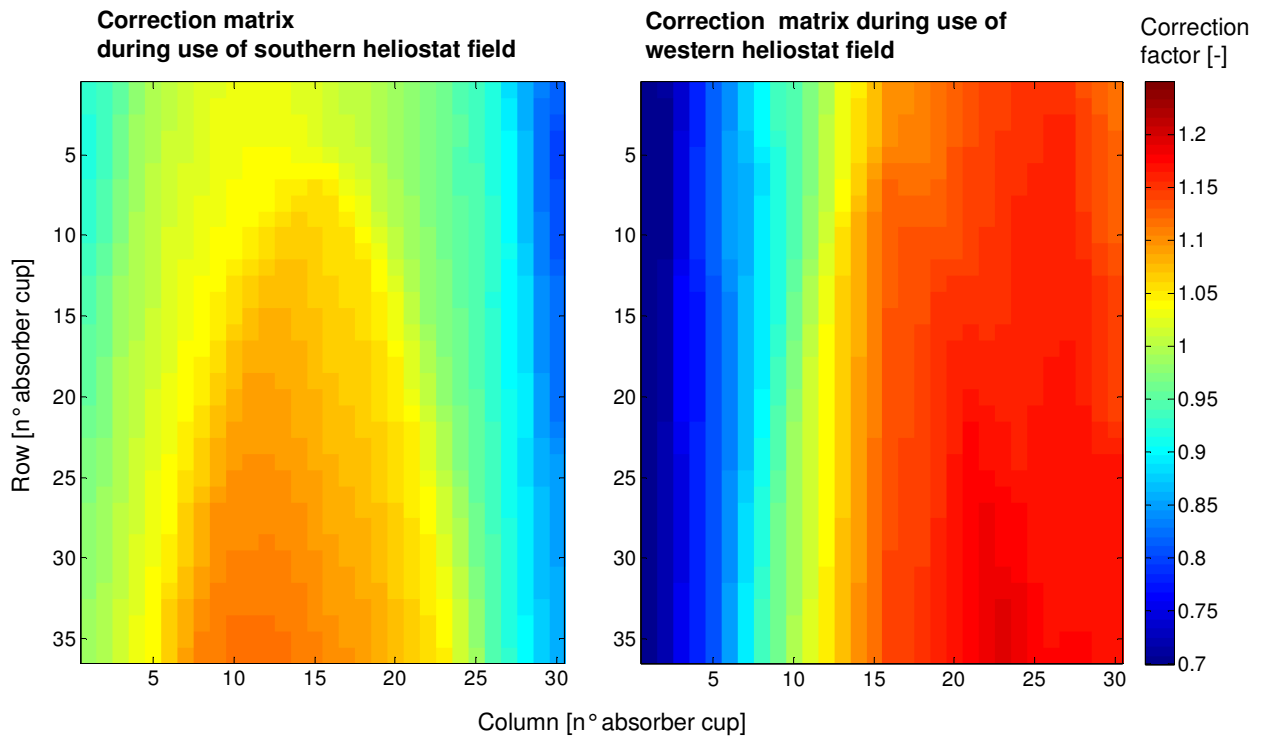


**Fig. 11: Different correction matrices**

Thus it can be derived that there is a significant influence by the shape of the heliostat field and the used heliostats during operation of the solar tower on the signal that arrives at the sensor of the CCD-camera and finally on the measured flux density and distribution. Depending on used heliostats a BRDF correction can be calculated live (i.e. while the solar tower is in operation) with the help of the determined BRDF values. For the calculation of the correction matrix, the assumption is made that each heliostat adds the same power to the whole incident power. Therefore the correction is not dependent on the actual sun position. Further work

will compare this against correction matrices that include cosine and atmospheric losses and uncertainties in heliostat tracking and aimpoint control and therefore have to be calculated for the exact time of the acquisition of the flux distribution.

After application of the ambient light and BRDF corrections to the raw intensities of the absorber cups (Fig. 12) the flux measured by the radiometer is used for absolute calibration of the data. As exposure times for the CCD-camera can easily be adjusted, measured flux is only limited by the measurement range of the radiometer used for the calibration.

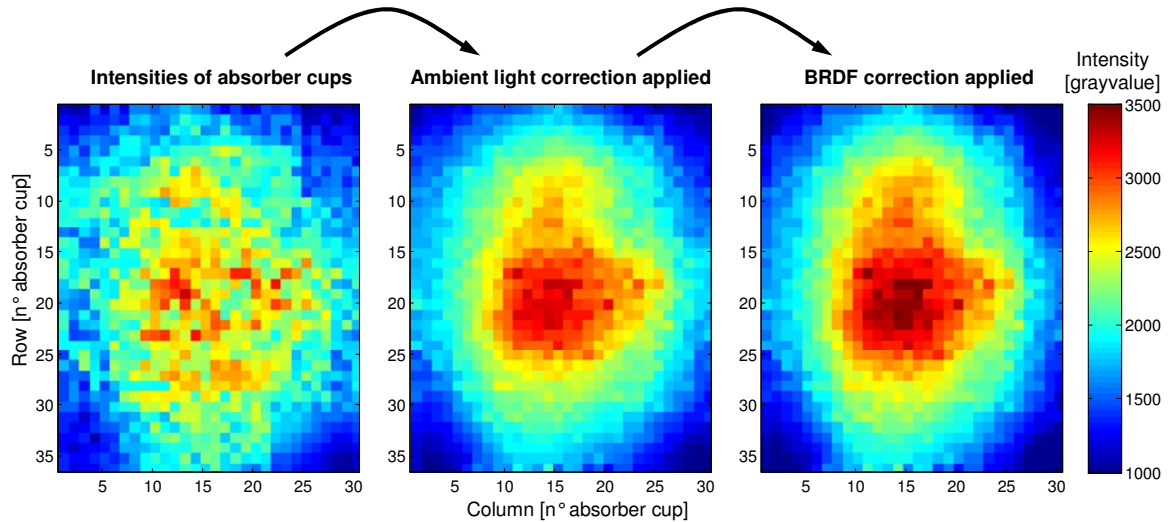


**Fig. 12: Application of ambient light and BRDF correction to the raw intensity map of a flux distribution matrix**

### 2.3 Results

The measurement system output of the MATLAB/Labview environment consists of the incident power onto the receiver and its four subreceivers, the region of maximum flux, and a flux distribution matrix with a resolution of individual absorber cups (15 cm x 15 cm).

As no other flux measurement system is installed at the receiver at STJ, the system had to be validated indirectly. Measured flux distribution was used as input for a dynamic simulation model that was developed at DLR [9]. Resulting simulated hot air enthalpies at the receiver outlets only differ by maximum 5 % from measured ones. Error analysis affirms that the measurement uncertainty for the incident power is below 5 %. Further work will be done to evaluate the resulting error in flux distribution after applying all mentioned corrections. A direct comparison to a moving bar measurement at the PSA is already planned for the near future. An evaluation of different flux density measurement systems has shown that especially for aimpoint control and continuous measurements the measurement on the external receiver surface is the preferable solution even though measurement uncertainties exist [8].

### 3. Conclusion & Outlook

An indirect flux measurement system was developed, tested and evaluated during operation at the Plataforma Solar de Almería and the Solar Tower Jülich. Results demonstrate the feasibility of the system and accurate measurement of flux density with fast response time and resolution only limited to the size of individual absorber cups. The system is comparatively low priced, freely scalable and can easily be adapted to external receivers with different aperture sizes, geometries and absorber surfaces. Refinement of the method will include cosine and atmospheric losses. Finally a simulation based BRDF correction using advanced raytracing tools and receiver models elaborated at DLR [9] will be developed and evaluated but results will depend very much on aiming precision and heliostat quality.



## Acknowledgments

Financial support from the German Federal Ministry for the Environment, Nature Conservation and Nuclear Safety, the Ministries of Economic Affairs of the States of North Rhine-Westphalia and Bavaria are gratefully acknowledged. We also thank Stadtwerke Jülich GmbH for operating the power plant and their support, Kraftanlagen München GmbH for supplying the STJ with coldfingers and radiometers and integrating them into the process control system and Markus Pfänder for his valuable contributions during the early development phase of this work.

## References

- [1] M. Röger, P. Herrmann, M. Ebert, C. Prah, S. Ulmer, F. Göhring, Flux density measurement on large-scale receivers, Proceedings of SolarPACES 2011, Granada, Spain, Sept. 20-23 (2011)
- [2] S. Pomp, P. Schwarzbözl, G. Koll, F. Göhring, T. Hartz, M. Schmitz, B. Hoffschmidt, The Solar Tower Jülich – First Operational Experiences and Test Results, Proceedings of 16<sup>th</sup> SolarPACES, Perpignan, France, Sep. 21-24, 2010
- [3] S. Ulmer, Messung der Strahlungsflussdichteverteilung von punktkonzentrierenden solarthermischen Kraftwerken, VDI-Verlag GmbH, Düsseldorf, 2004
- [4] European Machine Vision Association: EMVA Standard 1288 – Standard for Characterization and Presentation of Specification Data for Image Sensors and Cameras (Release A1.03), 2006
- [5] E. Lüpfer, P. Heller, Steffen Ulmer, R. Monterreal, J. Fernández, Concentrated solar radiation measurement with video image processing and online fluxgauge calibration. Solar Thermal 2000 International Conference Sydney, Australia, March 8-10 (2000)
- [6] R. Siegel, J. R. Howell, Wärmeübertragung durch Strahlung, Springer-Verlag, Berlin, 1988
- [7] J. Gengenbach, REM-Berechnung und Messung des Emissionsgrades mikrostrukturierter Oberflächen, Helmut-Schmidt-Universität, Universität der Bundeswehr Hamburg, 2007
- [8] Belhomme, B., Pitz-Paal, R., Schwarzbözl, P., Ulmer, S., New Fast Ray Tracing Tool for High-Precision Simulation of Heliostat Fields, Journal of Solar Energy Engineering, 131, 3 (2009), 031002-031008.
- [9] N. Ahlbrink, J. Anderson, M. Diehl, D. Maldonado Quinto, R. Pitz-Paal, Optimized Operation of an Open Volumetric Air Receiver, Proceedings of 16<sup>th</sup> SolarPACES, Perpignan, France, Sep. 21-24, 2010